

Received: 2018.09.13
Accepted: 2019.01.02
Published: 2019.05.27

Biomechanical Effect of an Exposed Dental Implant's First Thread: A Three-Dimensional Finite Element Analysis Study

Authors' Contribution:
Study Design A
Data Collection B
Statistical Analysis C
Data Interpretation D
Manuscript Preparation E
Literature Search F
Funds Collection G

ABCDEF 1 **Malik Ismail Hudieb**
ACF 2 **Noriyuki Wakabayashi**
DEF 3,4 **Osama Abdullah Abu-Hammad**
ADE 5 **Shohei Kasugai**

1 Department of Preventive Dentistry, Faculty of Dentistry, Jordan University of Science and Technology, Irbid, Jordan
2 Department of Removable Partial Prosthodontics, Graduate School of Medical and Dental Sciences, Tokyo Medical and Dental University, Tokyo, Japan
3 Department of Removable Prosthodontics, Faculty of Dentistry, University of Jordan, Amman, Jordan
4 College of Dentistry, Taibah University, Al-Madinah Al-Munawarah, Saudi Arabia
5 Oral Implantology and Regenerative Dental Medicine, Graduate School, Tokyo Medical and Dental University, Tokyo, Japan

Corresponding Author: Malik Ismail Hudieb, e-mail: mihudieb@just.edu.jo
Source of support: Departmental sources

Background: The purpose of this study was to assess the effect of different exposure levels of a dental implant's first thread on adjacent bone stress and strain using the finite element analysis method.





Material/Methods: Three-dimensional models of 2 threaded implants and abutments with a mandibular bone segment were constructed to represent the covered (C) and exposed models. In the exposed models, the implant was first placed in the bone, and rotated around its axis a quarter-turn each time to simulate 4 different levels of first thread exposure at the mid-lingual side: Upper Flank (UF), Thread Crest (TC), Lower Flank (LF), and Thread Root (TR) models. Oblique forces were applied and analysis was performed.

Results: Maximum compressive stress magnitude and distribution varied according to the exposed thread profile. In the exposed group, peak stress ranged from 136 MPa to 197 MPa in TC and LF models, respectively, compared to 141 MPa in C model. In LF, UF, and C models, peak stress was observed at the mid-lingual side of the crestal region, while in TC and TR models, peak stress shifted distally in accordance with thread profile. However, alveolar bone volumes which exhibited compressive microstrain levels within the physiological loading and maintenance windows were relatively close in all models.

Conclusions: Results suggest that the exposed thread profile influences stress and strain outcomes in the adjacent bone; however, this influence is only limited to a small region around the exposed thread.

MeSH Keywords: **Alveolar Bone Loss • Dental Implants • Finite Element Analysis**

Full-text PDF: <https://www.medscimonit.com/abstract/index/idArt/913186>

 2235  3  4  32



Background

Dental implants have been successfully used in recent decades [1,2]. Different implant designs have been developed and utilized since the introduction of osseointegrated dental implants [3,4]. Threaded dental implant designs have been found to enhance primary stability, increase the bone-implant contact area, and help dissipate interfacial stress [5].

Adequate available bone dimensions in the horizontal and vertical directions are considered as a prerequisite for successful and predictable implant treatment [6]. However, continuous bone resorption usually takes place following tooth extraction [7,8]. Implant placement in these ridges might result in crestal bone dehiscence defects with uncovered implant neck and/or exposed crestal threads for threaded implants [9,10]. Consequently, an esthetic problem is expected, especially in the anterior area first, and later the situation might be complicated with peri-implantitis or peri-implant mucosites [11,12]. Management of such exposed threads ranges from leaving them uncovered [10] to intentionally inclining the implants to avoid thread exposure [13], and/or covering them with bone graft and/or membrane according to the guided bone regeneration (GBR) techniques [14,15].

Because of their oscillating and spiral profile, different levels of thread exposure can result in different geometries at the crestal region. Considering the nature of the osseointegrated contact between the implant and the surrounding bone, the local anatomy and the geometry of the peri-implant bone were found to influence the distribution and intensity of the generated stress in the surrounding bone [16,17]. In fact, excessive stress generated around dental implants are considered as one of the main causes of peri-implant bone loss and/or implant failure [18,19]. Dental implant success and survival studies have frequently utilized the first crestal thread as a reference for bone resorption in the first year of loading [20].

Several methods have been used to evaluate the biomechanical aspect of dental implants, including finite element analysis (FEA), photoelastic materials, and strain gauges. However, FEA is a numerical method that has been widely used to evaluate mechanical parameters of the implant, prosthesis, bone, and related structures [16].

The effect of the exposed implant's thread at the crestal bone has not been evaluated in relation to the generated stress in the peri-implant bone structures. Therefore, the aim of this study was to assess the biomechanical effects of several patterns of first thread exposure compared to the non-exposed thread, using finite element method (FEM).

Material and Methods

Finite element models

Three-dimensional (3D) finite element models representing a mandibular alveolar bone segment and dental implant were modeled using FEA software (ANSYS13.0, ANSYS, Inc., PA) (Figure 1A). For the bone model, a 3D segment of a mandibular bone was created based on the most common morphologic model for the mandibular premolar region in our previous study [21]. CT scan-based average dimensions of outer cortical bone outline at the premolar region were used to create x and y plots. The resulting area made from this outline comprised an outer 1.5-mm-thick cortical bone layer cancellous core. The two-dimensional image on the x-y plane was then extruded in the z axis to construct the 3D model with 15 mm in the mesio-distal length. The maximum bucco-lingual width and the vertical dimension of the mandible model at the first premolar region where the implant is placed were 13.9 mm and 28.6 mm, respectively.

A standard dental implant model with 4-mm diameter and 10-mm intraosseous length was constructed with standard v-shaped spiral threads with thread pitch and thread height of 0.8 mm and 0.4 mm, respectively [22,23]. To mimic the covered and the exposed crestal thread models, threaded profile started from the uppermost crestal point (platform) in the exposed models, while in the covered model, threads were shifted 0.8 mm apically down to preserve the intraosseous implant length (Figure 1B). In the exposed models, the implant was vertically placed in the alveolar ridge; it was rotated then around its long axis a quarter-turn each time to produce several exposure levels of the first thread at the mid-lingual peri-implant bone. Four different possibilities resulted in 4 exposed models: Upper Flank (UF), Thread Crest (TC), Lower Flank (LF), and Thread Root (TR), according to which the outer cortical bone plate approached the implant at the crest tip of the first thread, the thread root, the middle of upper thread flank, and middle of the lower thread flank, respectively (Figure 1C). The other implant model, in which threads shifted apically, represented the control/covered model (CN) with the first crestal thread fully impeded in the alveolar bone (Figure 1C). Finally, a 5.5-mm-high simplified abutment was constructed and connected to the implants.

Loading and boundary conditions

The material properties of cancellous and cortical bones were modeled as being transversely isotropic and linearly elastic [5,24], which describes an anisotropic material. The materials of the implant and the abutment were considered as isotropic and linearly elastic (Table 1).

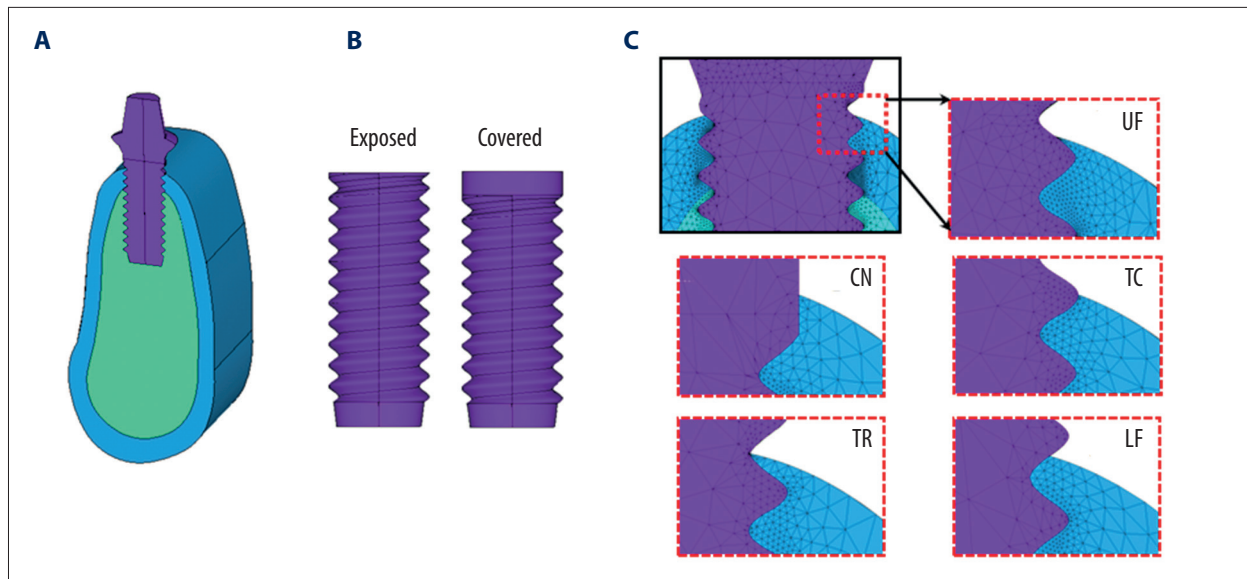


Figure 1. The bone segment with implant and abutment models (A). The implant models (B): Exposed model, in which threads started from the crestal region and Non-Exposed model in which threads were shifted down. Meshed FE images (C) of the crestal region of the implant and the cortical bone in the 5 models, CN – control (covered), UF – upper flank, LF – lower flank, TC – thread crest, and TR – thread root.

Table 1. Material properties used in of this study [5,22].

	Young's modulus (E, MPa)		Poisson's ratio		Shear modulus (G, MPa)	
Cortical bone	Ex	12 600	Vxy	0.300		
			Vyz	0.253	Gxy	4850
	Ey	12 600	Vxz	0.253		
			Vyx	0.300	Gyz	5700
	Ez	19 400	Vzy	0.390		
			Vzx	0.390	Gxz	5700
Cancellous bone	Ex	1148	Vxy	0.055		
			Vyz	0.010	Gxy	68
	Ey	210	Vxz	0.322		
			Vyx	0.010	Gyz	68
	Ez	1148	Vzy	0.055		
			Vzx	0.322	Gxz	434
Titanium	107 000		0.300			

The bone models were constrained in all directions at the distal and mesial surface nodes. The implants were rigidly anchored in the bone models along the entire interface. A static load of 200N was directed to the center of the occlusal surface of the abutment 30° oblique to the buccal, which corresponded with the direction of occlusal forces in the premolar region [25]. The resultant load

(200N) was used to simulate the average maximum occlusal load for fixed partial prosthesis supported by implants in the premolar region [25]. The maximum compressive stress and strain magnitudes and distribution along with the volumetric distribution of the compressive strain [26] were analyzed and calculated for the cortical and cancellous bones in the 5 models.

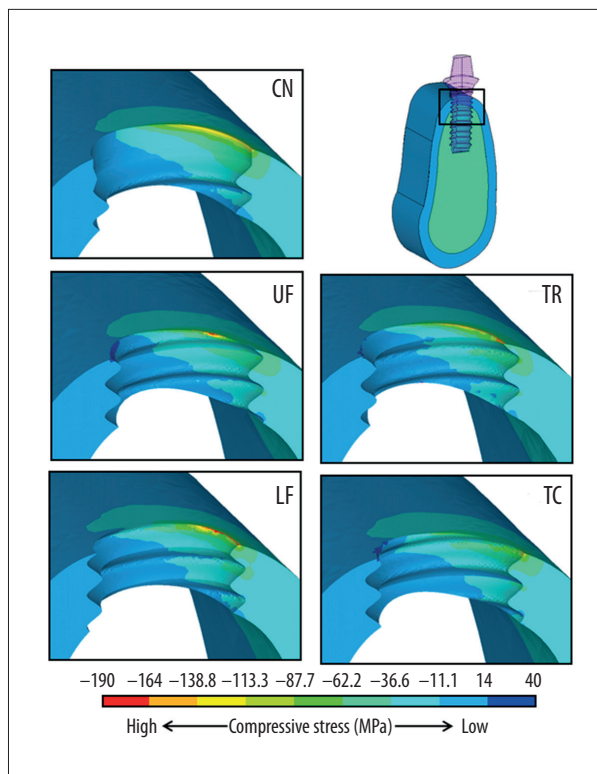


Figure 2. The effects of different levels of thread exposure (UF, TR, LF, and TC) compared to the control/covered threads model (CN). The figure on the upper left indicates the viewing angle and force direction (red arrow). Models are sectioned halves and viewed from the mesial side. The same contour scale was used for all models. The red area represents the highest compressive stress.

Results

The peak stress and strain values and large-strain bone volume in all models are shown in Table 2. The distributions of the compressive stress in the peri-implant cortical bone in the 5 models are shown in Figure 2.

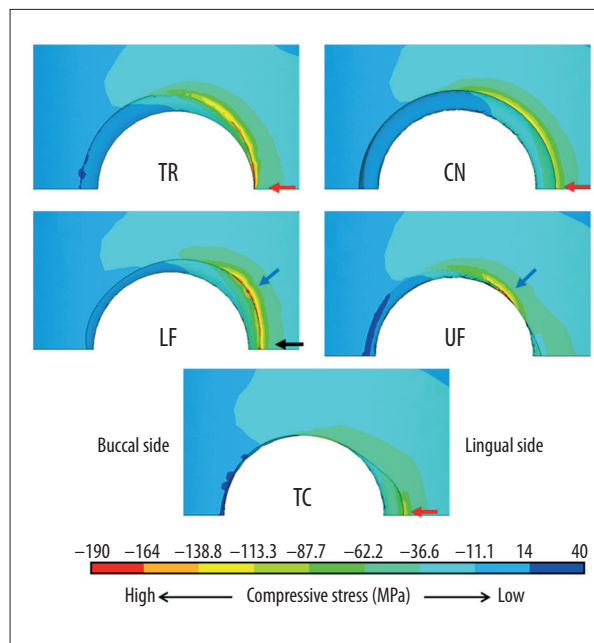


Figure 3. The compressive stress distribution in the cervical cortical bone for the 5 models. The distal half of each model is viewed from the top. Each contour graphic was divided into 9 parts, with different colors according to the stress level, shown in a scale below each figure. Red arrows indicate the location of the maximum compressive stress that appeared at the mid-lingual side in TC, TR, and CN models. The black arrow in LF model indicates a high compressive stress (but not the maximum) at the mid-lingual side. Blue arrows indicate the location of the maximum compressive stress that appeared in the vicinity of the exposed thread and deviated from the mid-lingual side in LF and UF models.

Peak compressive stress

Regarding the peak stress results (Table 2), the highest peak compressive stress in the cortical bone was noted in the LF model, with -197.32 MPa, while the lowest value was in the TC model, with -136.74 MPa. In the cancellous bone, peak stress

Table 2. Maximum compressive stress and strain in the cortical and cancellous parts of the bone for each model.

Model	Compressive stress (MPa)		Compressive strain (μ strain)	
	Cortical	Cancellous	Cortical	Cancellous
TC	-136.74	-1.97	-8910	-7150
TR	-149.67	-1.90	-9110	-7650
UF	-192.82	-1.42	-10 290	-5430
LF	-197.32	-1.46	-11 810	-6840
CN	-141.56	-1.64	-8430	-6360

Table 3. Compressive strain volumes (mm³).

Model	Cortical bone volumes (mm ³)			Cancellous bone volumes (mm ³)		
	200–2500 $\mu\epsilon$	2500–4000 $\mu\epsilon$	>4000 $\mu\epsilon$	200–2500 $\mu\epsilon$	2500–4000 $\mu\epsilon$	>4000 $\mu\epsilon$
TC	262.79	0.74	0.066	857.35	2.26	0.043
TR	266.16	0.82	0.103	843.39	2.86	0.281
UF	263.86	0.86	0.034	835.21	2.75	0.078
LF	264.22	0.76	0.082	841.84	2.74	0.251
CN	258.76	0.70	0.038	822.39	2.49	0.107

Cortical and cancellous bone volumes exhibited compressive strain that represent maintenance (200–2500 $\mu\epsilon$), physiological loading (2500–4000 $\mu\epsilon$), and pathological overloading (>4000 $\mu\epsilon$) for each model.

magnitudes were significantly lower than those in the cortical bone, with a range of –1.96 MPa in the TC model to –1.42 MPa in the UF model.

Distribution of the compressive stress

The maximum stress was noted at the peri-implant cervical cortical bone in the exposed and covered models; however, the location of the peak compressive stress around the implant neck varied in the 5 models (Figure 3). In the C, TC, and TR models, the peak stress was observed at the mid-lingual region of the implant's neck, but in LF and UF models it was shifted to the disto-lingual side. However, in the cancellous bone, the maximum stress was located just beneath the lingual side of the crestal cortical bone plate in TC and TR models, while in the C, UF, and LF models, maximum stress shifted apically away from the crestal region.

Volumetric analysis of the compressive strain results

The peri-implant cortical bone volumes exhibited a compressive strain level above 4000 μ strain ranged from 0.034 mm³ in the UF model to 0.102 mm³ in the TR model (Table 3). However, for the compressive strain ranges 2500–4000 and 200–2500 μ strain, the volumes were close in the 5 models. Likewise, bone volumes of strain ranges in the cancellous bone were found to be close for different thread exposure levels.

Discussion

Exposure of crestal thread has been found to influence the distribution and magnitude of the peak compressive stress and strain generated in the peri-implant bone.

Upon loading the implants, maximum compressive stress has been noted at the crestal region of the cortical bone in exposed and covered thread models, and this might be attributed

for the difference of materials strength [27]. However, a high stress concentration was observed at the mid-lingual region in the C, TC, TR, and LF models, representing the peak stress in the C, TC, and TR models, while the peak stress was located on the disto-lingual side, corresponding to the point where the lower flank passes to the curved thread crest in the LF model, and where the upper flank passes to the curved thread root in the UF model. It can be generally observed that the distribution of the generated peak stress in the surrounding crestal bone is influenced by the relative position of the thread root or crest to the outer cortical bone contour (Figure 4 curves).

The highest maximum compressive stress was found in the LF model, where the crestal region at the lingual side is subjected to the direct forces under the lower flank of the first thread, while the lowest was in the TC model, where most of the crestal region at the lingual side was located over the upper flank, providing a favorable contact angle for the bone-implant interface [26].

Regarding the volumetric analysis of the strain level, compressive strain thresholds of the mechanostat theory [28–30] were applied in this study (Table 3). The cortical bone volume exhibited pathological overloading compressive strain level (above 4000 μ strain), which was larger in the TR model. This might be because the crestal bone contour was always under the lower flank of the first thread in this model (Figures 2, 3). However, very close results were obtained in all models for the windows thresholds of maintenance (200–2500), physiological loading (2500–4000), and pathological overloading (above 4000 μ strain) in the cancellous bone, and for the maintenance and physiological loading in the cortical bone.

Treatment of crestal thread exposure might range from leaving them exposed [10], tilting the implants to avoid the exposure of crestal threads [13], or covering exposed threads utilizing suitable GBR technique. However, inclining dental implants according to the angulation of available bone only might affect

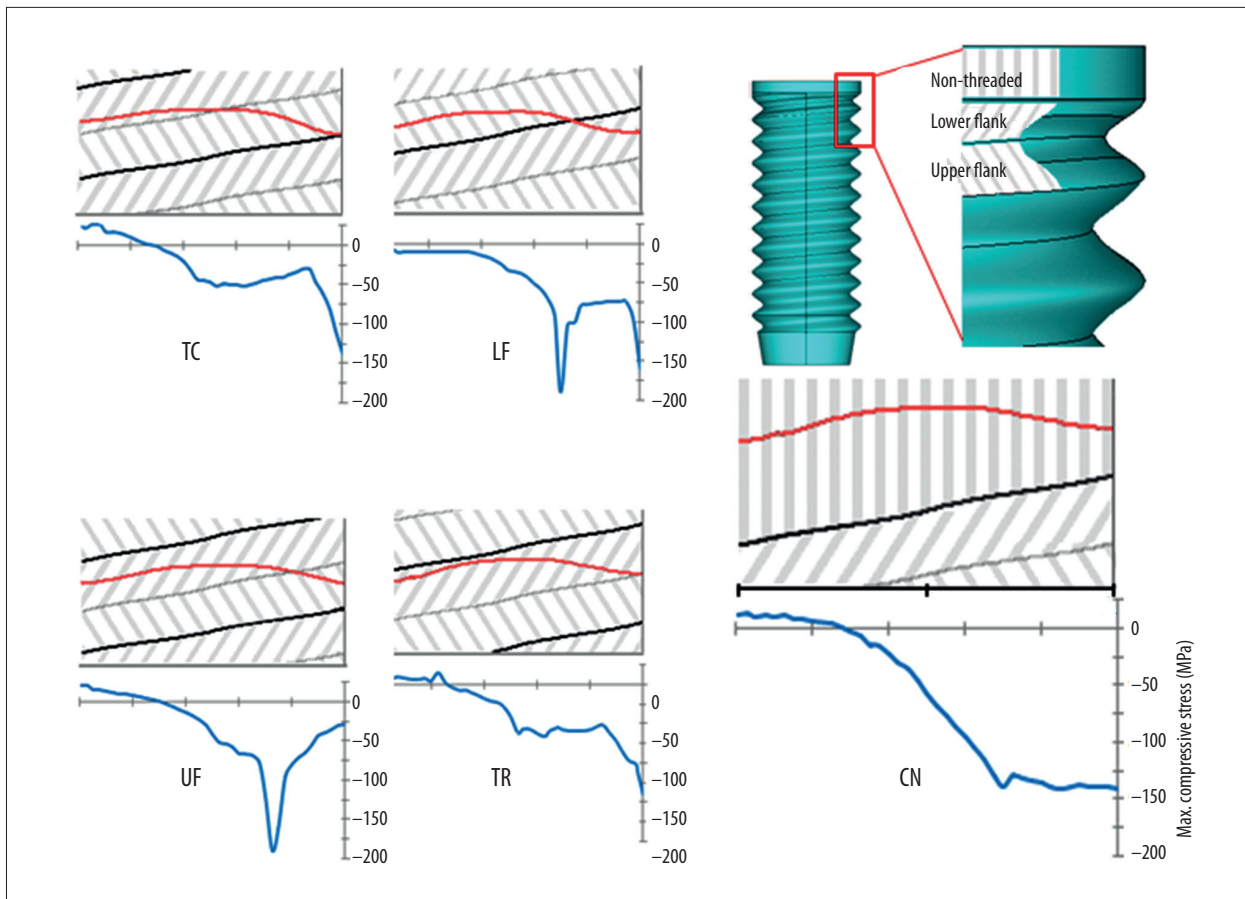


Figure 4. Compressive stress profiles (blue color) at the distal half of the crestal region around the implant starting from mid-lingual side (L) to mid-buccal side (B) and plotted with the crestal bone contour (red line in the upper panel for each model). The upper right graph indicates the non-threaded, upper, and lower flanks used in upper panels. For each model, the upper panel represents the crestal bone level (in relation to the thread's crests (black line) and roots (gray line). Upper and lower flanks are represented as tilted background. Vertical gray lines represent the non-threaded region in the non-exposed model (CN).

the loading conditions, as implants might be subjected to larger off-axis forces, which have very destructive effects on the implant-bone assembly [3]. On the other hand, covering the exposed threads with bone graft and/or membrane treatment option have been described and used in clinical and animal studies, including the use of autografts, BioOss, and ePT-FE membrane. However, taking into consideration the risk of complications and failure, these resource-demanding procedures might not represent the treatment of choice, especially if no esthetic problem resulted. Moreover, the biomechanical advantages of such procedures might be doubtful, as reported by Rasmussen et al. [31], who used resonance frequency and removal torque measurements, and demonstrated that fully covered implants after using membrane induced bone augmentation did not show significantly better stability results compared to the exposed thread implants [31].

The results of the current analysis revealed that exposed dental implant crestal thread will only influence the local

distribution of the generated stress and strain around the exposed implant thread, and may not affect the overall biomechanical performance of the dental implants supporting previous clinical studies [9].

The level of crestal thread exposure along with the adjacent bone geometry depend largely on implant site preparation, implant neck design, and residual bone morphology. While it might be difficult to control the level of thread exposure, implants should be placed with caution because sharp edges at the crestal region may result. These sharp edges, as in the TR model (Figure 1), might be associated with local stress and strain concentrations [31].

Several studies have addressed the biomechanical aspect of dental implants; however, implant models were mostly constructed as a non-threaded cylinder, which may not represent the real morphology of dental implants. Moreover, when threaded implants are used, axysymmetric models are mostly

constructed [16]. However, spiral implants have been used [5], and in this study, spiral implants were constructed in order to accurately analyze the generated peri-implant bone stress and strain.

Our present results also show the importance of mechanical parameters used to judge the performance of dental implants in this field. For example, although the same implant was used for the 4 exposed thread models in this study, an increase of 43% of the peak stress was observed when the implant was revolved around its axis (LF and TC models). This might demonstrate the impact of local interface morphology of the bone and implant at the crestal region on the maximum generated stress results [17,32].

While incomplete coverage of implant threads may result at the crestal region because of the curved nature or the narrow dimension of the alveolar bone, in this study, a well-developed bone model was used to establish a baseline with which future analysis with different bone morphologies will be compared.

Advantages of the FEA over other biomechanical analysis methods include the realistic mode of approach and the accuracy

of results; however, limitations should be highlighted. In this study, the implant-bone interface was modeled on the assumption of a perfect bonding, as no detachment was allowed under tensile or shear stresses. This was assumed because the interfacial shear and tensile strengths at the bone-implant interface have not been determined. Also, cyclic fatigue loading rather than the static forces should be considered if a structural model was made to account for changes in the bone-implant interface with degradation or failure of osseointegration.

Conclusions

Within the limitations of this study, an exposed implant's first thread level was found to influence the distribution and magnitude of the generated peak compressive stress on adjacent bone. However, the effect of the exposed thread profile was found to be limited to a small region localized at the crestal bone around the implant neck.

Conflict of interest

None.

References:

1. Hultin M, Gustafsson A, Klinge B: Long-term evaluation of osseointegrated dental implants in the treatment of partly edentulous patients. *J Clin Periodontol*, 2000; 27(2): 128–33
2. Ferrigno N, Laureti M, Fanali S, Grippaudo G: A long-term follow-up study of non-submerged ITI implants in the treatment of totally edentulous jaws. Part I: Ten-year life table analysis of a prospective multicenter study with 1286 implants. *Clin Oral Implants Res*, 2002; 13(3): 260–73
3. Falco A, Berardini M, Trisi P: Correlation between implant geometry, implant surface, insertion torque, and primary stability: *In vitro* biomechanical analysis. *Int J Oral Maxillofac Implants*, 2018; 33(4): 824–30
4. Huang HL, Hsu JT, Fuh LJ et al: Biomechanical simulation of various surface roughnesses and geometric designs on an immediately loaded dental implant. *Comput Biol Med*, 2010; 40: 525–32
5. Huang HL, Chang CH, Hsu JT et al: Comparison of implant body designs and threaded designs of dental implants: A 3-dimensional finite element analysis. *Int J Oral Maxillofac Implants*, 2007; 22: 551–62
6. Lekholm U, Adell R, Lindhe J et al: Marginal tissue reactions at osseointegrated titanium fixtures. (II) A cross-sectional retrospective study. *Int J Oral Maxillofac Surg*, 1986; 15: 53–61
7. Eufinger H, König S, Eufinger A: The role of alveolar ridge width in dental implantology. *Clin Oral Investig*, 1997; 1: 169–77
8. Cawood JI, Howell RA: A classification of the edentulous jaws. *Int J Oral Maxillofac Surg*, 1988; 17: 232–36
9. Veltri M, Ferrari M, Balleri P: One-year outcome of narrow diameter blasted implants for rehabilitation of maxillas with knife-edge resorption. *Clin Oral Implants Res*, 2008; 19: 1069–73
10. Lekholm U, Sennerby L, Roos J, Becker W: Soft tissue and marginal bone conditions at osseointegrated implants that have exposed threads: A 5-year retrospective study. *Int J Oral Maxillofac Implants*, 1996; 11: 599–604
11. Figuro E, Graziani F, Sanz I et al: Management of peri-implant mucositis and peri-implantitis. *Periodontol* 2000, 2014; 66(1): 255–73
12. Wang WC, Lagoudis M, Yeh CW, Paranhos KS: Management of peri-implantitis – A contemporary synopsis. *Singapore Dent J*, 2017; 38: 8–16
13. Mattsson T, Kondell PA, Gynther GW et al: Implant treatment without bone grafting in severely resorbed edentulous maxillae. *J Oral Maxillofac Surg*, 1999; 57: 281–87
14. Veis AA, Tsirlis AT, Parisis NA: Effect of autogenous harvest site location on the outcome of ridge augmentation for implant dehiscences. *Int J Periodontics Restorative Dent*, 2004; 24: 155–63
15. Hurzeler MB, Kohal RJ, Naghshbani J et al: Evaluation of a new bioresorbable barrier to facilitate guided bone regeneration around exposed implant threads. An experimental study in the monkey. *Int J Oral Maxillofac Surg*, 1998; 27: 315–20
16. Geng JP, Tan KB, Liu GR: Application of finite element analysis in implant dentistry: A review of the literature. *J Prosthet Dent*, 2001; 85: 585–98
17. Holmes DC, Loftus JT: Influence of bone quality on stress distribution for endosseous implants. *J Oral Implantol*, 1997; 23: 104–11
18. Duyck J, Ronold HJ, Van Oosterwyck H et al: The influence of static and dynamic loading on marginal bone reactions around osseointegrated implants: An animal experimental study. *Clin Oral Implants Res*, 2001; 12: 207–18
19. Kim Y, Oh T-J, Misch CE, Wang H-L: Occlusal considerations in implant therapy: Clinical guidelines with biomechanical rationale. *Clin Oral Implants Res*, 2005; 16: 26–35
20. Kong L, Liu BL, Hu KJ: [Optimized thread pitch design and stress analysis of the cylinder screwed dental implant.] *Huaxi Kouqiang Yixue Zazhi*, 2006; 24: 509–12, 515 [in Chinese]
21. Hudieb M, Wakabayashi N, Suzuki T, Kasugai S: Morphologic classification and stress analysis of the mandibular bone in the premaxillary region for implant placement. *Int J Oral Maxillofac Implants*, 2010; 25: 482–90
22. Ma P, Liu HC, Li DH et al: Influence of helix angle and density on primary stability of immediately loaded dental implants: Three-dimensional finite element analysis. *Zhonghua Kouqiang Yixue Zazhi*, 2007; 42: 618–21
23. Petrie CS, Williams JL: Comparative evaluation of implant designs: influence of diameter, length, and taper on strains in the alveolar crest. A three-dimensional finite-element analysis. *Clin Oral Implants Res*, 2005; 16: 486–94
24. O'Mahony AM, Williams JL, Spencer P: Anisotropic elasticity of cortical and cancellous bone in the posterior mandible increases peri-implant stress and strain under oblique loading. *Clin Oral Implants Res*, 2001; 12: 648–57
25. Mericske-Stern R, Assal P, Mericske E, Burgin W: Occlusal force and oral tactile sensibility measured in partially edentulous patients with ITI implants. *Int J Oral Maxillofac Implants*, 1995; 10: 345–53

26. Hudieb MI, Wakabayashi N, Kasugai S: Magnitude and direction of mechanical stress at the osseointegrated interface of the micro-thread implant. *J Periodontol*, 2011; 82: 1061–70
27. Arinc H: Effects of prosthetic material and framework design on stress distribution in dental implants and peripheral bone: A three-dimensional finite element analysis. *Med Sci Monit*, 2018; 24: 4279–87
28. Frost HM: The mechanostat: A proposed pathogenic mechanism of osteoporoses and the bone mass effects of mechanical and nonmechanical agents. *Bone Miner*, 1987; 2: 73–85
29. Mosley JR, Lanyon LE: Strain rate as a controlling influence on adaptive modeling in response to dynamic loading of the ulna in growing male rats. *Bone*, 1998; 23: 313–18
30. Frost HM: From Wolff's law to the mechanostat: A new "face" of physiology. *J Orthop Sci*, 1998; 3: 282–86
31. Rasmusson L, Meredith N, Sennerby L: Measurements of stability changes of titanium implants with exposed threads subjected to barrier membrane induced bone augmentation. An experimental study in the rabbit tibia. *Clin Oral Implants Res*, 1997; 8: 316–22
32. Nagasao T, Kobayashi M, Tsuchiya Y et al: Finite element analysis of the stresses around fixtures in various reconstructed mandibular models – part II (effect of horizontal load). *J Craniomaxillofac Surg*, 2003; 31: 168–75